Received June 10, 2019, accepted June 27, 2019, date of publication July 4, 2019, date of current version July 24, 2019.

Digital Object Identifier 10.1109/ACCESS.2019.2926858

Suppression of Intensity and Frequency Noise at Low-Sensitivity Operating Points of Period-One Dynamics of Optically Injected Semiconductor Lasers

MOHAMMAD A. ALMULLA[1], (Member, IEEE), AND JIA-MING LIU[2], (Fellow, IEEE)
[1]Department of Electrical Engineering, Kuwait University, Safat 13060, Kuwait
[2]Department Electrical and Computer Engineering, University of California at Los Angeles, Los Angeles, CA 90095, USA

Corresponding author: Mohammad A. Almulla (almulla@ucla.edu)

ABSTRACT Period-one (P1) dynamics induced by an optically injected semiconductor laser oscillate at microwave frequencies. The oscillation frequency of a P1 dynamic can be rendered nearly insensitive to small-signal parameter fluctuations and intrinsic laser noise at appropriate operating conditions of the master and slave lasers. In this paper, the noise-canceling properties of the various low-sensitivity (LS) operating points is demonstrated through their dependency on the noise fluctuation frequency and power. The three different types of LS operating points show their effectiveness in suppressing not only P1 intensity and frequency fluctuations caused by narrowband laser perturbations but also intensity and frequency noise caused by broadband intrinsic and extrinsic noise sources.

INDEX TERMS Microwave photonics, nonlinear dynamics, optical injection, period-one dynamics, semiconductor lasers.

I. INTRODUCTION

Period-one (P1) dynamics are self-sustained intensity oscillations that can be induced by proper optical injection of a semiconductor laser. These limit-cycle oscillations emerge at critical operating points through a Hopf bifurcation due to undamped relaxation resonances of the semiconductor laser [1], [2]. They are invoked by a cost-effective, all-optical configuration with innate single-sideband characteristics and are frequency-tunable reaching up to ten times the relaxation resonance frequency of the uninjected solitary laser [3]. These favorable characteristics attracted considerable attention, resulting in extensive research in the last two decades. Numerous applications using the P1 dynamics have been demonstrated in optical signal processing [4]–[6], optical communication [7], [8], and optical detection [9], [10]. The P1 dynamics have been examined in several types of semiconductor lasers subject to external optical injection, including quantum-well distributed feedback lasers (DFBs) [3], [11], vertical-cavity surface-emitting lasers (VCSELs) [12], quantum-dot lasers [13], quantum cascade lasers [14], and nano-lasers [15].

The P1 oscillations generated by semiconductor lasers under optical injection suffer from poor spectral purity due to spontaneous emission noise. Compared with other techniques to generate photonic microwaves [16], the P1 oscillations have broad microwave linewidths of the order of 1–100 MHz [17]. Furthermore, the fluctuations in the operating conditions of the master and slave lasers cause considerable microwave frequency jitters and frequency hopping [18]. The poor stability of a P1 oscillation diminishes its appeal through reduction of the signal-to-noise ratio in optical communication applications, degradation in the noise performance in signal processing applications, and limitation in the detection range in optical ranging applications. Therefore, many efforts have been conducted to improve the P1 oscillation stability. A reference microwave source at the P1 oscillation frequency or its subharmonics can double lock the P1 oscillation through direct current modulation [19] or external optical modulation [20], [21]. To eliminate the reference microwave source, an electronic microwave amplifier and an attenuator are added to form an optoelectronic feedback loop,

The associate editor coordinating the review of this manuscript and approving it for publication was San-Liang Lee.

reducing the P1 microwave linewidth by three orders of magnitude [22], [23]. To bypass the bandwidth-limiting electronics, an all-optical polarization-rotated optical feedback approach was demonstrated, showing microwave stabilization of P1 dynamics at high frequencies, although an order of magnitude less than the optoelectronic feedback scheme [18]. To suppress the time-delay side peaks, an all-optical dual-loop optical feedback was also demonstrated [24].

Recently, P1 oscillations with low-sensitivity to intrinsic and extrinsic perturbations on the laser have been identified [25]–[28]. By properly choosing the operating conditions, the nonlinear effects are exploited to mitigate the perturbation-induced noise in the system. Three types of low-sensitivity (LS) operating points are identified: low sensitivity to injection-strength fluctuations (LS_ξ), low sensitivity to detuning-frequency fluctuations (LS_f), and low sensitivity to bias-current fluctuations ($LS_{\tilde{J}}$). A particular LS operating point is identified at a local P1 frequency extremum with respect to the corresponding operating parameter. At an LS_ξ operating point, injection strength fluctuations emerging from temperature and/or bias-current variations in the master and slave lasers are minimized. Detuning frequency fluctuations emerging from temperature and/or bias-current variations in the master and slave lasers are minimized at an LS_f operating point. Current variations of the slave laser are suppressed at a P1 minimum with respect to the bias current at an $LS_{\tilde{J}}$ operating point. These LS operating points can further enhance on the stabilization techniques described above. For example, the LS operation can reduce the microwave frequency jitters due to path-length fluctuation and can reduce the emerging delay time side-peaks of a P1 oscillation under the optical feedback stabilization scheme mentioned above [18], [29]. Furthermore, the LS operation can also enhance the P1 dynamic performance in generating frequency-modulated continuous wave (FMCW) and microwave frequency comb signals [29]–[31]. Therefore, it is important to understand the capabilities of the various LS points of operation in suppressing system fluctuation noise for optimum P1 performance. Depending on the dominant source of the system fluctuation noise, the various LS operating points can be exploited for the different P1 frequency applications.

In this work, through detailed numerical calculations, demonstration of the noise-cancelling properties of the LS operation of P1 oscillations are analyzed for different noise intensities and frequencies. To mimic fluctuations in the temperature and bias current of the master and slave lasers, modulation on the injection strength, detuning frequency, or bias current is applied. The amplitude of the emerging modulation sidebands normalized to the P1-frequency amplitude manifest the stability of the operating points against the fluctuations of a specific parameter. The modulation sideband responses in the power spectrum and optical spectrum represent the response of the circulating optical power to the fluctuation noise, whereas the modulation sideband response in the carrier spectrum represents the response of the gain medium to the fluctuation noise. The effectiveness of the LS operating points in suppressing not only P1 intensity and frequency fluctuations caused by narrowband intrinsic laser perturbations but also intensity and frequency noise caused by broadband intrinsic and extrinsic noise sources is illustrated. The LS_ξ and $LS_{\tilde{J}}$ operating points respectively show vulnerability to the fluctuation strengths of the injection strength and bias current, limiting the suppression bandwidth to around 1 GHz. The LS_f operating points, by contrast, is mainly limited by the fluctuation frequency of the detuning frequency.

This paper is organized as follows: Section II describes the theoretical model used to simulate the characteristics of the optical field, power spectra and carrier spectra of an optically injected semiconductor laser. The main results are presented in Section III, showing the characteristics of the three types of LS operating points against fluctuation noise. Finally, Section IV concludes the paper by summarizing the results and discussing their implications.

II. THEORETICAL MODEL

The nonlinear dynamics of an optically injected semiconductor laser with modulation on the injection strength, detuning frequency, or bias current can be described by a set of coupled equations relating the intracavity optical field amplitude to the carrier density of the injected laser [32]. For numerical calculations, these quantities are normalized where a_r and a_i represent the real and imaginary parts of the normalized complex field amplitude, respectively, and $\tilde{n}$ is the normalized carrier density [33]:

$$\frac{da_r}{dt} = \frac{1}{2}\left[\frac{\gamma_c\gamma_n}{\gamma_s\tilde{J}}\tilde{n}\,(a_r+ba_i)-\gamma_p\left(a_r^2+a_i^2-1\right)(a_r+b'a_i)\right] +\xi\left[1+m_\xi\cos(2\pi f_\xi t)\right]\gamma_c\cos(2\pi ft+m_f\sin(2\pi f_f t)) \quad (1)$$

$$\frac{da_i}{dt} = \frac{1}{2}\left[\frac{\gamma_c\gamma_n}{\gamma_s\tilde{J}}\tilde{n}\,(-ba_r+a_i)-\gamma_p\left(a_r^2+a_i^2-1\right)(-b'a_r+a_i)\right] -\xi\left[1+m_\xi\cos(2\pi f_\xi t)\right]\gamma_c\sin(2\pi ft+m_f\sin(2\pi f_f t)) \quad (2)$$

$$\frac{d\tilde{n}}{dt} = -\left[\gamma_s+\gamma_n\left(a_r^2+a_i^2\right)\right]\tilde{n}-\gamma_s\tilde{J}\left(a_r^2+a_i^2-1\right) +\frac{\gamma_s\gamma_p}{\gamma_c}\tilde{J}\left(a_r^2+a_i^2\right)\left(a_r^2+a_i^2-1\right) +\gamma_s m_{\tilde{J}}(1+\tilde{J})\cos(2\pi f_{\tilde{J}}t) \quad (3)$$

The experimentally determined laser parameters used in this paper are those from an InGaAsP/InP DFB laser with a cavity decay rate of $\gamma_c = 5.36\times10^{11}$ s^{-1}, a spontaneous carrier relaxation rate of $\gamma_s = 5.96\times10^9$ s^{-1}, a differential carrier relaxation rate of $\gamma_n = \tilde{J}\cdot6.162\times10^9$ s^{-1}, a nonlinear carrier relaxation rate of $\gamma_p = \tilde{J}\cdot1.563\times10^{10}$ s^{-1}, a linewidth enhancement factor of $b = 3.2$, and a gain saturation factor of $b' = 3.2$ [34]. The normalized bias current, normalized injection strength, and detuning frequency are $\tilde{J}$, ξ, and f, respectively. The modulation indices $m_{\tilde{J}}$, m_ξ, and m_f, and

modulation frequencies $f_{\tilde{J}}$, f_{ξ}, and f_f represent modulation on the bias current, injection strength, and detuning frequency, respectively.

Equations (1)–(3) are solved using a second-order Runge-Kutta integration for a duration of 1.25 μs for each time series with an integration time step of 2.4 ps. The Fourier transform of the resulting time series are calculated to find the optical and power spectra of the slave laser output. The relaxation rates γ_n and γ_p vary linearly with the normalized bias current; therefore, as $\tilde{J}$ is changed the linear dependency must be taken into account in the theoretical model [35].

The noise-cancelling properties of the P1 oscillation frequency induced by an optically injected semiconductor laser are influenced by fluctuations in the temperature and bias currents, as well as the random disturbances from spontaneous emission noise and charge-carrier noise, in the slave and master lasers. Fluctuating source terms with contributions to the optical-field and carrier-density equations could be introduced to account for spontaneous emission of the slave laser. However, the $LS_{\tilde{J}}$, LS_f, or LS_{ξ} operation suppresses P1 noise caused only by bias-current, detuning-frequency, or injection-strength fluctuations, respectively, while spontaneous emission noise and charge-carrier noise of the lasers still play a role in the P1 noise. The carrier-density equation contribution from the charge-carrier noise is eliminated at an $LS_{\tilde{J}}$ point, yet the field-equation contribution from the spontaneous emission still exists at an $LS_{\tilde{J}}$ point. Similarly, only the frequency contribution of the spontaneous emission in the field-equation is eliminated at an LS_f, and only the amplitude contribution is eliminated at an LS_{ξ} operating point. Therefore, in investigating the effects of noise, we do not formulate the model by incorporating noise terms in each equation. Instead, we consider the specific fluctuations one by one. The noise source terms in the optical-field and carrier-density equations are thus neglected in the model so that the contribution from a specific operational-parameter fluctuation is solely considered.

To show the influence of a specific fluctuation noise on an LS operating point, the corresponding modulation source term is applied. The $m_{\tilde{J}}$ and m_{ξ} modulation indices are varied from 1% to 10% while m_f is varied from 0.1 to 2. The modulation frequencies $f_{\tilde{J}}$, f_{ξ}, and f_f are varied from 100 MHz to 2 GHz.

III. RESULTS AND ANALYSES

A. EFFECTS OF FLUCTUATION NOISE ON THE LOW-SENSITIVITY OPERATING POINTS

The P1 oscillation frequency induced by optical injection can be tuned by simply varying one of the operating parameters. Applying modulation on the P1 frequency generates two sidebands around the P1 frequency in the power spectra, at positive and negative offsets from the P1 frequency. The amplitudes of the modulation sidebands relative to the P1 frequency amplitude represent the stability of the P1 frequency against system fluctuations at a specific intensity and frequency. The positive and negative modulation sideband responses represent the response of the circulating optical field with respect to a specific perturbation. Therefore, to analyze the noise-cancelling properties around an LS_{ξ}, LS_f, or $LS_{\tilde{J}}$ point, the depth, width, and prominence of the positive and negative modulation sideband responses are investigated for various modulation strengths and modulation frequencies.

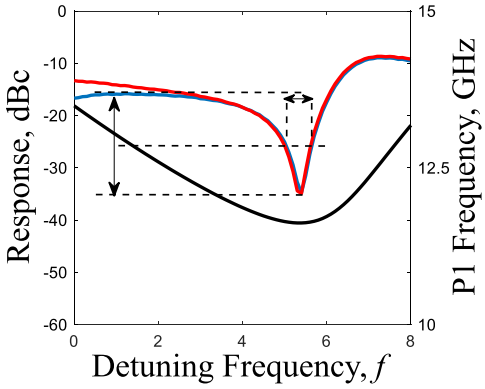

FIGURE 1. A representative LS_f operating point obtained by applying a weak modulation at 500 MHz on the detuning frequency at fixed $\xi = 0.065$ and $\tilde{J} = 1.222$. The responses of the positive (blue) and negative (red) modulation sidebands show dips around a local minimum of the P1 frequency (black) with respect to the detuning frequency. The vertical double-headed arrows represent the prominence, whereas the horizontal double-headed arrow represents the width of the prominence. Note that the width of a prominence is defined at the half of the prominence dip on the dBc scale, not as the 3dB width at the half of the prominence on a linear scale.

Figure 1 shows a set of representative responses of the positive and negative modulation sidebands around a P1 frequency minimum when detuning-frequency modulation is applied. The dips in the modulation sideband responses represent the maximum amount of noise suppression at an LS operating point around a P1 frequency minimum with respect to the fluctuating operational parameter. The prominence of the modulation sideband responses is represented by the depths of the modulation sidebands relative to their respective highest points in proximity of the P1 frequency minimum. The proximity of the P1 frequency minimum is defined as $\pm 30\%$, $\pm 100\%$, $\pm 20\%$ away from the point where the P1 frequency is minimized for the injection strength, detuning frequency, and bias current, respectively. For the operating points used, deviating at a higher percentage away from the P1 frequency minimum drives the laser out of the P1 dynamic region and into either the stable locking or complex dynamic region. The prominence is a measure of the significance of the dips in the modulation sideband responses at an LS operating point relative to the surrounding background response around a P1 frequency minimum. A high prominence indicates pronounced dips in the responses of the positive and negative modulation sidebands; by contrast, a low prominence indicates dull dips in the modulation sideband responses. The prominence is shown as a vertical double-headed arrow in Fig. 1. To characterize the noise-cancelling bandwidth as

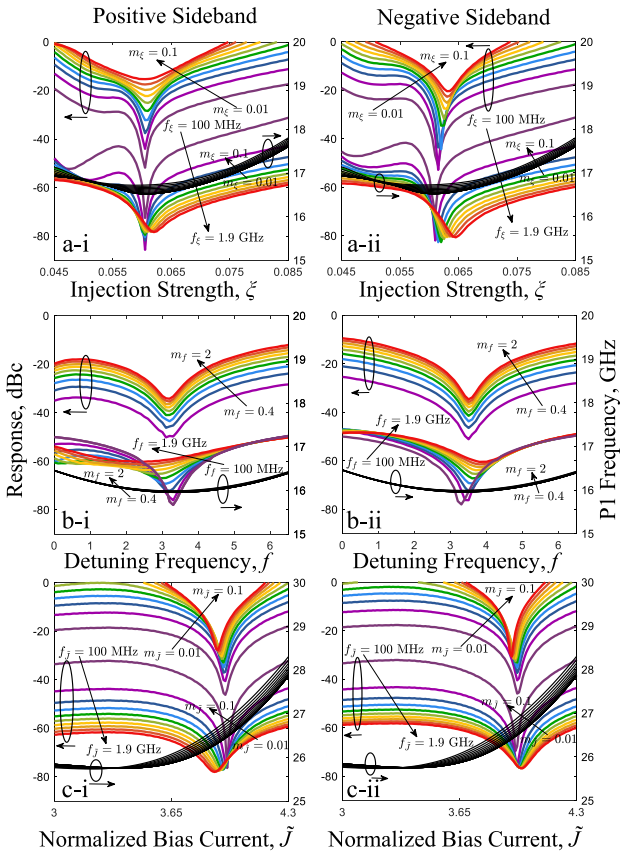

FIGURE 2. Responses of the positive (left column) and negative (right column) modulation sidebands around a P1 frequency minimum (black) at (a) an LS_ξ operating point with fixed $f = 10$ GHz and $\tilde{J} = 2.8$, (b) an LS_f operating point with fixed $\xi = 0.1$ and $\tilde{J} = 1.222$, and (c) an $LS_{\tilde{J}}$ operating point with fixed $\xi = 0.15$ and $f = 17$ GHz. Upper curves show modulation responses as the modulation strength is varied for a fixed modulation frequency of 500 MHz. The modulation responses as the modulation frequency is varied for fixed modulation strengths of $m_\xi = 0.01$, $m_f = 0.8$, and $m_{\tilde{J}} = 0.01$ are offset by –30 dB and shown as lower curves in (a), (b), and (c), respectively.

the operational parameters are tuned away from the P1 frequency minimum, the width of the prominence in terms of the deviations of the operating parameters $\Delta\xi$, Δf, and $\Delta\tilde{J}$ from the LS operating point is calculated. Note that the width of a prominence, shown as the horizontal double-headed arrow in Fig. 1, is defined at the half of the prominence dip on the dBc scale. It is not defined as the 3dB width at the 3dB point that corresponds to the half of the prominence dip on a linear scale; the reason is that the 3dB width is so narrow that adjusting an injection parameter to be within the 3dB width is much more difficult than keeping it to be within the prominence width defined in Fig. 1. Therefore, in this paper, the term ''half-prominence'' refers to a point at half of the prominence dip on the dBc scale, not that on a linear scale. This point will be further discussed at the end of this subsection.

Figures 2(a), 2(b), and 2(c) respectively show the positive (left column) and negative (right column) modulation sideband responses around a P1 frequency minimum when either the modulation strength or the modulation frequency is fixed at an LS_ξ, LS_f, and $LS_{\tilde{J}}$ point. For clarity, the modulation sideband responses when the modulation strength is fixed are offset by –30 dB and shown in the lower colored curves in Fig. 2.

Figure 2(a) shows an LS_ξ operating point at the local minimum of the P1 frequency where the injection strength is swept from $\xi = 0.045$ to $\xi = 0.085$, while the other operating parameters are held constant at $f = 10$ GHz and $\tilde{J} = 2.8$. For a fixed modulation frequency of $f_\xi = 500$ MHz and weak modulation strengths, pronounced dips in the positive and negative modulation sidebands are observed at the P1 frequency minimum. As the modulation strength is increased from $m_\xi = 0.01$ to $m_\xi = 0.1$ at 0.01 increments, the dips in the responses of the modulation sidebands are progressively reduced. This reduction in the responses of the modulation sidebands indicates that for a significantly strong fluctuation in the injection strength, intensity noise suppression at an LS_ξ operating point is no longer achieved. This behavior is demonstrated in the upper parts of Figs. 2(a-i) and 2(a-ii) for the positive and negative sidebands, respectively. For a fixed modulation strength of $m_\xi = 0.01$ and a low modulation frequency, pronounced modulation sideband responses in both the positive and negative modulation sidebands are observed at the P1 frequency minimum. As the modulation frequency is increased from $f_\xi = 100$ MHz to $f_\xi = 1.9$ GHz at 200 MHz increments, the dips in responses of the modulation sidebands are still maintained but with reduced prominent features. This frequency-dependent reduction in the prominent features of the responses indicates that at a high modulation frequency of the injection strength, noise suppression at an LS_ξ operating point is similar to that at other operating points in the proximity of the P1 frequency minimum. This behavior is demonstrated in the lower parts of Figs. 2(a-i) and 2(a-ii) for the positive and negative modulation sidebands, respectively. For small modulation strengths and low modulation frequencies, the dips in the responses of the positive and negative modulation sidebands are at the point where the P1 frequency is at a local minimum. For large modulation strengths or high modulation frequencies the dips in the responses of the positive and negative modulation sidebands are slightly offset to larger injection strengths away from the point where the P1 frequency is minimized.

Figure 2(b) shows an LS_f operating point at a local minimum of the P1 frequency, where the detuning frequency is swept from $f = 0$ GHz to $f = 6$ GHz while the other operating parameters are held constant at $\xi = 0.1$ and $\tilde{J} = 1.222$. For a fixed modulation frequency of $f_f = 500$ MHz and small modulation strengths, dips in the responses of the positive and negative modulation sidebands are observed at the P1 frequency minimum. As the modulation strength is increased from $m_f = 0.4$ to $m_f = 2$ at 0.2 increments, the responses of the modulation sidebands maintain their prominent features while the response dips are progressively reduced. The preservation in the response of the modulation sidebands indicates that at such modulation strengths the LS_f operating point noise-cancelling properties are not

disturbed. This behavior is demonstrated in the upper part of Figs. 2(b-i) and 2(b-ii) for the positive and negative modulation sidebands, respectively. For a fixed modulation strength of $m_f = 0.8$ and a low modulation frequency, pronounced dips in the responses of the positive and negative modulation sidebands are observed at the P1 frequency minimum. As the modulation frequency is increased from $f_f = 400$ MHz to $f_f = 2$ GHz at 200 MHz increments, the dips in responses of the modulation sidebands are progressively reduced. The reduction in the responses of the modulation sidebands indicates that for a sufficiently high fluctuation in the detuning frequency, noise suppression at an LS_f operating point is no longer achieved. This behavior is demonstrated in the lower parts of Figs. 2(b-i) and 2(b-ii) for the positive and negative modulation sidebands, respectively. For small modulation strengths and low modulation frequencies, the dips in the responses of the positive and negative modulation sidebands are at the point where the P1 frequency is minimized. For high modulation frequencies, the dips in the responses of the positive and negative modulation sidebands are offset to lower and higher detuning frequencies, respectively.

Figure 2(c) shows an $\mathrm{LS}_{\tilde{J}}$ operating point at a local minimum of the P1 frequency, where the normalized bias current is swept from $\tilde{J} = 3.5$ to $\tilde{J} = 4.3$ while the other operating parameters are held constant at $\xi = 0.15$ and $f = 17$ GHz. For a fixed modulation frequency of $f_{\tilde{J}} = 500$ MHz and small modulation strengths, pronounced dips in the responses of the positive and negative modulation sidebands are observed at the proximity to where the P1 frequency is minimized. As the modulation strength is increased from $m_{\tilde{J}} = 0.01$ to $m_{\tilde{J}} = 0.1$ at 0.01 increments, the dips in the responses of the modulation sidebands are progressively reduced. The reduction in the responses of the modulation sidebands indicates that for a sufficiently strong fluctuation in the bias current, noise suppression at an $\mathrm{LS}_{\tilde{J}}$ operating point is no longer achieved. This behavior is demonstrated in the upper parts of Figs. 2(c-i) and 2(c-ii) for the positive and negative modulation sidebands, respectively. For a fixed modulation strength of $m_{\tilde{J}} = 0.01$ and a low modulation frequency, pronounced dips in the responses of the positive and negative modulation sidebands are observed at the P1 frequency minimum. As the modulation frequency is increased from $f_{\tilde{J}} = 100$ MHz to $f_{\tilde{J}} = 1.9$ GHz at 200 MHz increments, the dips in responses of the positive and negative modulation sidebands are still maintained but with less prominent features. The reduced prominent features of the responses indicate that at a high fluctuation frequency of the bias current, noise suppression at an $\mathrm{LS}_{\tilde{J}}$ operating point is similar to that at other operating points in the proximity of the P1 frequency minimum. This behavior is demonstrated in the lower parts of Fig. 2(c-i) and 2(c-ii) for the positive and negative sidebands, respectively. For small modulation strengths and low modulation frequencies, the dips in the responses of the positive and negative modulation sidebands are at proximity to the point where the P1 frequency is minimized. For high modulation frequencies, the dips in the responses of the positive and negative modulation sidebands are offset to lower and higher bias currents, respectively.

The offsets in the positive and negative modulation sideband responses when the modulation index is increased is related to the shift in the P1 frequency minimum. The P1 frequency around the LS operating points slightly shifts to higher frequencies as the modulation index is increased, as illustrated in the black curves in Fig. 2. By contrast, for each LS operating point, the P1 frequency is unchanged as the modulation frequency is varied. The offsets of the dips in the positive and negative modulation sidebands is a consequence of the anitguidance effect of the laser and is attributed to the parameters that relate the gain to the refractive index of the laser [33]. Therefore, the frequency dependencies of the LS operating points on the modulation strength can be used to measure the intrinsic parameters of the semiconductor laser [36].

A few remarks should be given to illustrate the reasoning behind the use of the prominence and its width at half-prominence as defined in Fig. 1 as the quantifiers of the LS operating points. The prominence is used to quantify the significance of the dips in the modulation sideband responses at an LS operating point relative to the surrounding background response around a P1 frequency minimum. Different LS operating points have different modulation sideband responses; therefore, the prominence is used to compare the different modulation sideband responses. If only the maximum suppression level is used, different modulation sideband responses would seem the same. For example, comparison of the $f_{\tilde{J}} = 100$ MHz response and $f_{\tilde{J}} = 1.9$ GHz response of Fig 2(c-i) show similar maximum suppression levels but different prominences. From a practical perspective, operating away from the maximum suppression points in the $f_{\tilde{J}} = 100$ MHz and $f_{\tilde{J}} = 1.9$ GHz responses results in different noise-cancelling properties. Therefore, the LS operating point at $f_{\tilde{J}} = 1.9$ GHz response is less significant than that at $f_{\tilde{J}} = 100$ MHz since the change in the response at $f_{\tilde{J}} = 1.9$ GHz is much less than that at $f_{\tilde{J}} = 100$ MHz when operating away from the maximum suppression point. The width at half-prominence as defined in Fig. 1 is used, rather than the 3dB width, to quantify the noise-cancelling bandwidth. The width at half-prominence measures the width relative to points much higher than 3 dB away from the maximum suppression point. At such points the amplitude of the modulation sidebands is still significantly less than the P1 amplitude, and the P1 dynamic is within low-sensitivity operation, as illustrated in Fig. 1. Consequently, the 3dB width is much narrower than the width at half-prominence. From a practical perspective, adjusting the injection parameters to be within the 3dB width is much more difficult than being within the width at half-prominence. For example, the half-prominence width defined on the dBc scale in Fig. 1 is around $\Delta f = 700$ MHz, yet the 3dB width is less than $\Delta f = 200$ MHz.

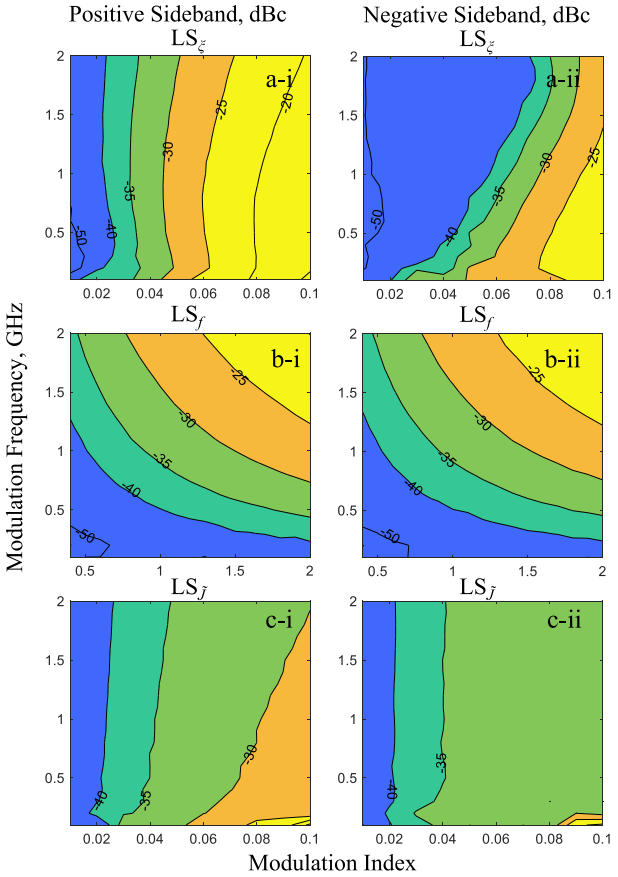

FIGURE 3. Mapping of the suppression level at the maximum suppression point in the modulation sideband response as a function of the modulation index and the modulation frequency for (a) the slave laser under optical injection with a varying injection strength but a fixed detuning frequency and a fixed bias current of $\xi = 0.045 - 0.085$, $f = 10$ GHz, and $\tilde{J} = 2.8$ at an LS$_\xi$ operating point, (b) the slave laser under optical injection with a varying detuning frequency but a fixed injection strength and a fixed bias current of $\xi = 0.1$, $f = 0 - 6$ GHz, and $\tilde{J} = 1.222$ at an LS$_f$ operating point, and (c) the slave laser under optical injection with a varying bias current but a fixed injection strength and a fixed detuning frequency of $\xi = 0.15$, $f = 17$ GHz, and $\tilde{J} = 3 - 4.5$ at an LS$_{\tilde{J}}$ operating point. The contour curves represent the maximum amount of sideband suppression with respect to the P1-frequency amplitude, in dBc, for the positive, column (i), and negative, column (ii), modulation sidebands.

B. MAPPING THE CHARACTERISTICS OF THE LOW-SENSITIVITY OPERATING POINTS

To demonstrate the noise-cancelling properties of the LS operating points, mappings of the response sideband suppression, the prominence, and the width at half-prominence for the positive and negative modulation sidebands are presented. The noise-cancelling properties of LS$_\xi$, LS$_f$, and LS$_{\tilde{J}}$ operating points are calculated when fluctuations in the injection strength, detuning frequency, and bias current are applied, respectively.

1) RESPONSE SIDEBAND SUPPERSION

Figure 3 shows mappings as a function of the modulation index and modulation frequency of the suppression in the positive (left column) and negative (right column) modulation sideband responses near a P1 frequency minimum. Figure 3(a) shows the level of maximum sideband suppression when the laser is under optical injection with a varying injection strength but a fixed detuning frequency and a fixed bias current of $\xi = 0.045$–0.085, $f = 10$ GHz, and $\tilde{J} = 2.8$, generating a P1 frequency near an LS$_\xi$ operating point. For small modulation strengths, suppression in modulation sidebands is observed even for high modulation frequencies, reaching 2 GHz. For large modulation strengths, the modulation sideband suppression is progressively reduced for increasing modulation frequencies. The maps in Figs. 3(a-i) and 3(a-ii) correspond to the dips in the responses of the positive and negative modulation sidebands shown in Figs. 2(a-i) and 2(a-ii), respectively.

Figure 3(b) shows the level of maximum sideband suppression when the laser is under optical injection with a varying detuning frequency but a fixed injection strength and a fixed bias current of $\xi = 0.1$, $f = 0 - 6$ GHz, and $\tilde{J} = 1.22$, generating a P1 frequency near an LS$_f$ operating point. For LS$_f$ operating points, the maximum sideband suppression is reduced as modulation frequency is increased. For low modulation frequencies, the modulation index has minimal effect on the point of maximum sideband suppression. The maps in Figs. 3(b-i) and 3(b-ii) correspond to the dips in the responses of the positive and negative modulation sidebands shown in Figs. 2(b-i) and 2(b-ii), respectively.

Figure 3(c) shows the level of maximum sideband suppression when the laser is under optical injection with a varying bias current but a fixed injection strength and a fixed detuning frequency of $\xi = 0.15$, $f = 17$ GHz, and $\tilde{J} = 3$–4.5, generating a P1 frequency near an LS$_{\tilde{J}}$ operating point. Similar to that seen at LS$_\xi$ operating points, modulation sideband suppression is observed even at high modulation frequencies. For large modulation strengths, the maximum sideband suppression is progressively reduced for the various modulation frequencies. The maps in Figs. 3(c-i) and 3(c-ii) correspond to the dips in the responses of the positive and negative modulation sidebands shown in Figs. 2(c-i) and 2(c-ii), respectively.

2) RESPONSE SIDEBAND PROMINENCE

To quantify the suppression in the positive and negative modulation sidebands in reference to the response away from the P1 frequency minimum, the prominence of each response curve is calculated. As illustrated in Fig. 1, the prominence of a modulation sideband response is calculated by finding the difference between the lowest point in the modulation sideband response relative to the highest point in proximity to the P1 frequency minimum, in dB. Figure 4 shows mappings, as a function of the modulation index and the modulation frequency, of the prominence in the responses of the positive (left column) and negative (right column) modulation sidebands near a P1 frequency minimum.

Figure 4(a) shows the prominence in the responses of the modulation sidebands when the laser is under optical injection with a varying injection strength but a fixed detuning frequency and a fixed bias current of $\xi = 0.045 - 0.085$,

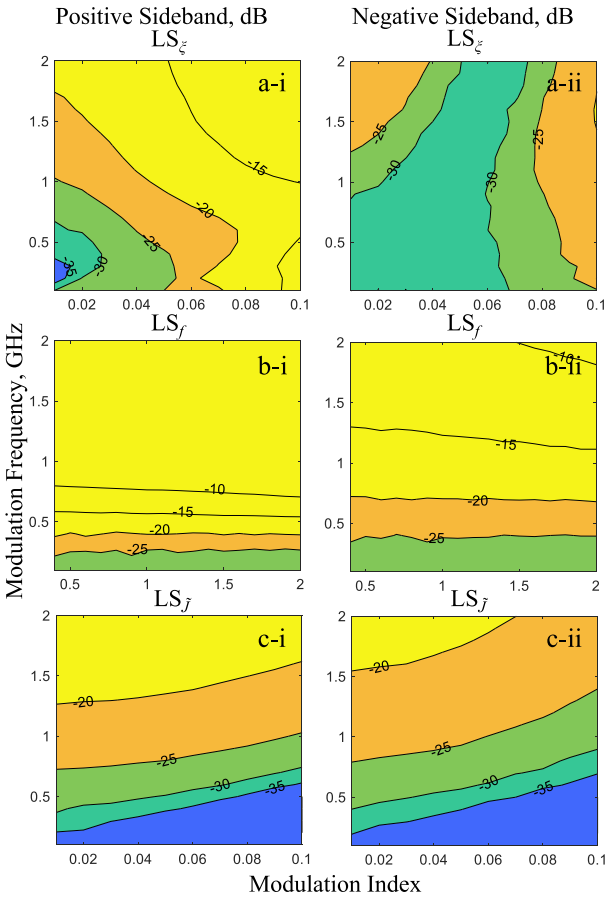

FIGURE 4. Mapping of the prominence in the responses of the modulation sidebands as a function of the modulation index and the modulation frequency for (a) the slave laser under optical injection with a varying injection strength but a fixed detuning frequency and a fixed bias current of $\xi = 0.045 - 0.085$, $f = 10$ GHz, and $\tilde{J} = 2.8$ at an LS$_\xi$ operating point, (b) the slave laser under optical injection with a varying detuning frequency but a fixed injection strength and a fixed bias current of $\xi = 0.1$, $f = 0 - 6$ GHz, and $\tilde{J} = 1.222$ at an LS$_f$ operating point, and (c) the slave laser under optical injection with a varying bias current but a fixed injection strength and a fixed detuning frequency of $\xi = 0.15$, $f = 17$ GHz, and $\tilde{J} = 3 - 4.5$ at an LS$_{\tilde{J}}$ operating point. The contour curves represent the depth of the modulation sideband response relative to the highest point in proximity to the P1 frequency minimum, in dB, for the positive, column (i), and negative, column (ii), modulation sidebands.

$f = 10$ GHz, and $\tilde{J} = 2.8$, generating a P1 frequency near an LS$_\xi$ operating point. For small modulation strengths and low modulation frequencies, high prominence is observed, as shown in Fig. 4(a). As either the modulation strength or the modulation frequency is increased, the prominence in the response of a modulation sideband is progressively reduced. The negative modulation sideband still shows a significantly high prominence even at high modulation frequencies and large modulation strengths. Therefore, simultaneous high prominence and pronounced dips in the responses of the positive and negative modulation sidebands indicating reduced sensitivity to fluctuations in the injection strength appear in the broad regions of small modulation strengths and low modulation frequencies. Figure 4(b) shows the prominence in the responses of the modulation sidebands when the laser is under optical injection with a varying detuning frequency but a fixed injection strength and a fixed bias current of $\xi = 0.1$, $f = 0 - 6$ GHz, and $\tilde{J} = 1.222$, generating a P1 frequency near an LS$_f$ operating point. The prominence in the responses of the positive and negative modulation sidebands is maintained as the modulation index is varied. By contrast, the prominence in the responses of the positive and negative modulation sidebands is progressively reduced as the modulation frequency is increased. Therefore, limited regions of LS$_f$ operation are found at low modulation frequencies, where simultaneous high prominence and pronounced dips in the responses of the positive and negative modulation sidebands are observed. Figure 4(c) shows the prominence in the responses of the modulation sidebands when the laser is under optical injection with a varying bias current but a fixed injection strength and a fixed detuning frequency of $\xi = 0.15$, $f = 17$ GHz, and $\tilde{J} = 3 - 4.5$, generating a P1 frequency near an LS$_{\tilde{J}}$ operating point. High prominence in the responses of the positive and negative modulation sidebands is observed regardless of the modulation strength. The high prominence in the region of strong modulation is attributed to strong modulation sidebands reaching amplitudes higher than the P1 frequency amplitude; therefore, strong modulation does not lead to reduced sensitivity. At high modulation frequencies, the prominence of the positive and negative modulation sidebands is progressively reduced. Therefore, simultaneous high prominence and pronounced dips in both the positive and negative modulation sidebands indicating reduced sensitivity to fluctuations in the bias current of the slave laser appear in the broad regions of small modulation strengths and low modulation frequencies.

3) RESPONSE SIDEBAND WIDTH AT HALF- PROMINENECE

To quantify the suppression width of an LS operating point, the widths at half-prominence in the responses of the positive and negative modulation sidebands are calculated. As illustrated in Fig. 1, the width at half-prominence of a modulation sideband response is calculated by finding the difference between the intersects of the response with the half-prominence line in terms of the varied control parameter.

Figure 5 shows mappings of the widths in the responses of the positive (left column) and negative (right column) modulation sidebands as a function of the modulation index and modulation frequency near a P1 frequency minimum. Figure 5(a) shows the width at half-prominence, in terms of $\Delta\xi$, of the modulation sideband responses when the laser is under optical injection with a varying injection strength but a fixed detuning frequency and a fixed bias current of $\xi = 0.045 - 0.085$, $f = 10$ GHz, and $\tilde{J} = 2.8$, generating a P1 frequency near an LS$_\xi$ operating point. In the regions of small modulation strengths and low modulation frequencies, the modulation response curves at the LS$_\xi$ operating point show narrow modulation sideband dips of $\Delta\xi < 0.005$. As the modulation strength or modulation frequency is increased, the modulation sideband responses show broad responses around the P1 frequency minimum.

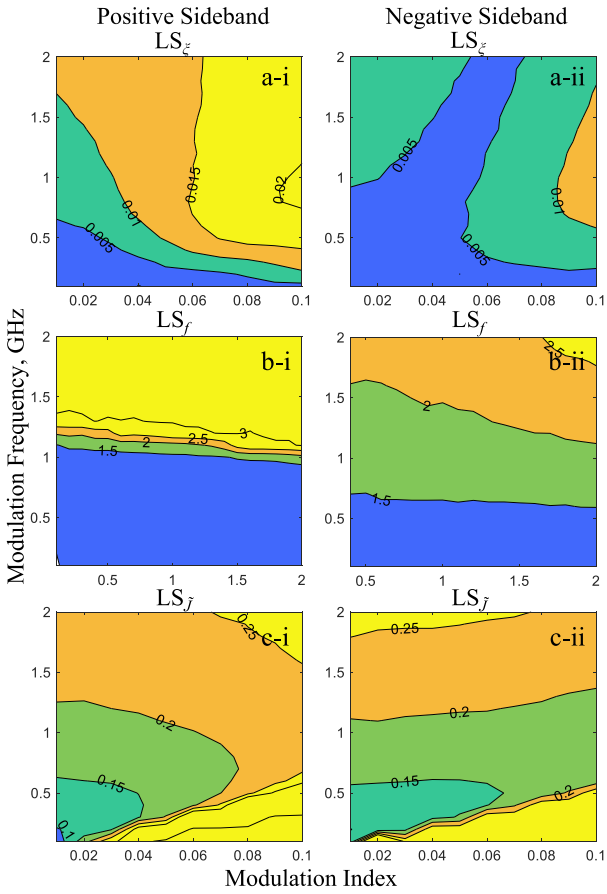

FIGURE 5. Mapping of the width in the response of the modulation sidebands as a function of the modulation index and the modulation frequency for (a) the slave laser under optical injection with a varying injection strength but a fixed detuning frequency and a fixed bias current of $\xi = 0.045 - 0.085$, $f = 10$ GHz, and $\tilde{J} = 2.8$ at an LS_ξ operating point, (b) the slave laser under optical injection with a varying detuning frequency but a fixed injection strength and a fixed bias current of $\xi = 0.1$, $f = 0 - 6$ GHz, and $\tilde{J} = 1.222$ at an LS_f operating point, and (c) the slave laser under optical injection with a varying bias current but a fixed injection strength and a fixed detuning frequency of $\xi = 0.15$, $f = 17$ GHz, and $\tilde{J} = 3 - 4.5$ at an $LS_{\tilde{J}}$ operating point. The contour curves represent the width at half-prominence of the modulation responses in proximity to the P1 frequency minimum, in terms of $\Delta\xi$, Δf, or $\Delta\tilde{J}$, for the positive, column (i), and negative, column (ii), modulation sidebands.

Comparison of Figs. 3(a), 4(a), and 5(a) shows that at LS_ξ operating points broadband intensity fluctuations are suppressed, reaching fluctuation frequencies of 1 GHz for weak intensity fluctuations.

Figure 5(b) shows the widths at half-prominence, in terms of Δf, of the modulation sideband responses when the laser is under optical injection with a varying detuning frequency but a fixed injection strength and a fixed bias current of $\xi = 0.1$, $f = 0 - 6$ GHz, and $\tilde{J} = 1.222$, generating a P1 frequency near an LS_f operating point. In the regions of low modulation frequencies, relatively narrow modulation sideband dips are observed with $\Delta f < 1.5$ GHz, regardless of the modulation index. Comparison of Figs. 3(b), 4(b), and 5(b) shows that at an LS_f operating point broadband frequency fluctuations are suppressed, reaching 500 MHz regardless of the fluctuation strength.

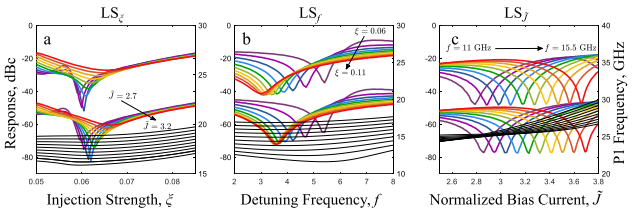

FIGURE 6. Responses of the positive and negative modulation sidebands around a P1 frequency minimum (black) at (a) an LS_ξ operating point with fixed $f = 10$ GHz and varying $\tilde{J} = 2.7 - 3.2$, (b) an LS_f operating point with fixed $\tilde{J} = 1.222$ and varying $\xi = 0.06 - 0.11$, and (c) an $LS_{\tilde{J}}$ operating point with fixed $\xi = 0.15$ and varying $f = 11 - 15.5$ GHz. Upper curves show the modulation responses of the positive modulation sideband; lower curves show the modulation responses of the negative modulation sidebands offset by −30 dB. The modulation strengths are fixed at $m_f = 0.8$ and $m_\xi = m_{\tilde{J}} = 0.01$ while the modulation frequencies are fixed at $f_\xi = f_f = f_{\tilde{J}} = 500$ MHz.

Figure 5(c) shows the widths at half-prominence, in terms of $\Delta\tilde{J}$, of the modulation sideband responses when the laser is under optical injection with a varying bias current but a fixed injection strength and a fixed detuning frequency of $\xi = 0.15$, $f = 17$ GHz, and $\tilde{J} = 3$–4.5, generating a P1 frequency near an $LS_{\tilde{J}}$ operating point. For small modulation strengths, narrow modulation sideband responses are observed with $\Delta\tilde{J} < 0.2$. Considerable increase in the width of the response is observed as the modulation index is slightly increased. Comparison of Figs. 3(c), 4(c), and 5(c) show that at an $LS_{\tilde{J}}$ operating point, broadband bias-current fluctuations are suppressed, reaching 1 GHz, for low fluctuation powers. As the fluctuation power is slightly increased, the noise suppression capabilities of the $LS_{\tilde{J}}$ are diminished.

C. EFFECTS OF OPERATING PARAMETERS ON THE LOW-SENSITIVITY OPERATING POINTS

The characteristics of the LS operating points do not only depend on the fluctuation strength and frequency of the fluctuating parameter but also on the operating conditions of the optical injection. The P1 frequency can be tuned by varying the injection strength, the detuning frequency, or the bias current, generating P1 frequency minima with respect to a specific operating parameter. Mappings of the various low sensitivity points showed different regions of LS operations for the laser under study [27]. Furthermore, under optical injection, the laser cavity configuration and the intrinsic properties of the semiconductor medium play a crucial role in the generated LS operating points [37].

Figure 6 shows the responses of the positive and negative modulation sidebands around a P1 frequency minimum when the modulation strength and the modulation frequency are fixed. For clarity, the curves for negative sideband responses are offset by –30 dB with respect to those of the positive sideband responses in each panel of this figure. Figure 6(a) corresponds to the LS_ξ operating point in Fig. 2(a). It shows the progression in the responses of the positive and negative modulation sidebands as the bias current is swept from $\tilde{J} = 2.7$ to $\tilde{J} = 3.2$ while the other operating parameters are held constant at $f = 10$ GHz, $m_\xi = 0.01$, and $f_\xi = 500$ MHz.

The minimum in the P1 frequency with respect to the injection strength originates at a point close to the chaotic dynamic region. The minimum in the P1 frequency with respect to the injection strength fades away as the bias current is increased to a point close to a Hopf bifurcation. By contrast, the positive and negative modulation sideband responses progressively reach a maximum point of suppression then fade away as the bias current is increased. This behavior is attributed to two competing nonlinear phenomena, the red-shifting of the cavity resonance and the Adler-type frequency pulling [25].

Figure 6(b) corresponds to the LS_f operating point in Fig. 2(b). It shows the progression in the responses of the positive and negative modulation sidebands as the injection strength is swept from $\xi = 0.06$ to $\xi = 0.11$ while the other operating parameters are held constant at $\tilde{J} = 1.222$, $m_f = 0.8$, and $f_f = 500$ MHz. Similar to the LS_ξ operating points in Fig. 6(a), the minimum in the P1 frequency with respect to the detuning frequency originates at a point close to the chaotic dynamic region. The minimum in the P1 frequency with respect to the injection strength fades away as the injection strength is increased to a point close to a Hopf bifurcation. The positive and negative modulation sideband responses progressively reach a maximum point of suppression then fade away as the injection strength is increased.

Figure 6(c) corresponds to the $LS_{\tilde{J}}$ operating point in Fig. 2(c). It shows the progression in the responses of the positive and negative modulation sidebands as the detuning frequency is swept from $f = 11$ GHz to $f = 15.5$ GHz while the other operating parameters are held constant at $\xi = 0.1$, $m_{\tilde{J}} = 0.01$, and $f_{\tilde{J}} = 500$ MHz. Similar to the LS_ξ and LS_f operating points in Figs. 6(a) and (b), the minimum in the P1 frequency with respect to the bias current originates at a point close to the chaotic dynamic region. The P1 frequency minimum shifts to lower bias currents as the detuning frequency is increased. However, unlike the LS_ξ and LS_f operating points in Figs. 6(a) and (b), the positive and negative modulation sideband responses are not completely suppressed and do not fade away as the P1 frequency minimum with respect to the bias current vanishes. This behavior is the same in different regions of the operating maps where a change in curvature of the P1 frequency minimum with respect to the bias current is observed. Bias-current modulation on the slave laser modulates the laser intensity and frequency because a change in the carrier density causes a change in the index of refraction of the laser medium which, in turn, generates frequency modulation. Therefore, the $LS_{\tilde{J}}$ points can be found at a local P1 extremum with respect to the bias current as well as at a P1 frequency extremum with respect to the detuning frequency. The operating point shown in Fig. 6(c) represents a P1 frequency extremum with respect to the detuning frequency showing simultaneous $LS_{\tilde{J}}$ and LS_f operating point.

The suppression, prominence, and width at half-prominence of the modulation sideband responses when the modulation strength and modulation frequency are varied at the various LS operating points represented in Fig. 6 have similar general characteristics as demonstrated in Figs. 3, 4, and 5, respectively.

The operating points that exhibit reduced sensitivity to a specific type of fluctuation noise show suppression in the response of the modulation sideband in the power spectrum. Similarly, suppression in the response of the modulation sideband in the carrier spectrum is observed for the various LS operating points. The suppression, prominence, and width at half-prominence in the responses of the carrier-spectrum modulation sidebands when the modulation strength and frequency are varied are similar to the behavior demonstrated in Figs. 3, 4, and 5, respectively. However, the modulation sidebands around the strong frequency components of the optical spectrum do not show simultaneous suppression in the modulation sideband responses at the various LS operating points. This suggests that the insensitivity arises from interference of the many frequency components in the optical spectrum suppressing the response of the gain medium and circulating optical field to the fluctuating parameter at an LS operating point [28].

IV. CONCLUSION

The noise-cancelling properties of the LS operation of P1 oscillations induced by optically injected semiconductor lasers have been analyzed. For different intensity- and frequency-fluctuation noise, the stability of the P1 oscillation against system parameter fluctuations are calculated through the amplitudes of the modulation sidebands relative to the P1 frequency amplitude, by modulating a specific operational parameter. Unlike phase noise measurements, this method allows the analysis of a specific noise contribution on the overall system. The suppression, prominence, and widths at half-prominence of the emerging modulation sideband responses at LS_ξ, LS_f, and $LS_{\tilde{J}}$ operating points demonstrate the stability of the P1 oscillation against injection-strength, detuning-frequency, and bias-current fluctuations, respectively.

The LS_ξ operating points are insensitive to fluctuations in the injection strength arising from intensity variations due to the fluctuations in the temperature and bias currents of the master and slave lasers. The P1-frequency insensitivity at LS_ξ operating points are highly susceptible to the strength of intensity fluctuations. The P1-frequency insensitivity to the fluctuations in the injection strength is no longer observed when the modulation strength is slightly increased. For weak intensity fluctuations, suppression of broadband intensity fluctuations at LS_ξ operating points reaching up to a fluctuation frequency of 1 GHz is verified. The LS_f operating points are insensitive to fluctuation in the detuning frequency arising from frequency variations due to the fluctuations in the temperature and bias currents of the master and slave lasers. The stability of the P1 frequency at LS_f operating points are highly susceptible to the system's frequency variation, showing a narrower bandwidth of suppression compared to the bandwidths at the other two types of LS operating points, reaching only 500 MHz. The $LS_{\tilde{J}}$ operating points are

insensitive to the fluctuations in the temperature of the slave and master lasers as well as to the fluctuations of the bias current of the slave laser but not the fluctuations of the bias current of the master laser. The stability of the P1 frequency at an $LS_{\tilde{J}}$ operating point shows a broader suppression bandwidth as compared to the other two types of LS operating points. All three types of LS operating points are located at proximity to points where the P1 frequency undergoes a frequency minimum with respect to the fluctuating parameter. The variations in the operational parameters also affect the LS characteristics although, regardless of the operating parameters, the LS operating points show similar trends as described above when changes in the fluctuation noise parameters are introduced.

The LS operating points are effective in suppressing specific small-signal, low-frequency fluctuations. Most intrinsic fluctuations that contribute to the noise of a semiconductor laser are low-frequency fluctuations. The main aspect of this work is to show the dependency of the LS operating points on the intensity and frequency of a specific noise term. Fluctuating source terms with contributions to the optical-field and carrier-density equations could be introduced to account for the spontaneous emission noise of the master and slave lasers. However, the $LS_{\tilde{J}}$, LS_f, and $LS_{\tilde{\xi}}$ operation respectively suppress only the noise caused by fluctuations in the bias current, the detuning frequency, and the injection strength of the slave laser, while spontaneous emission noise and charge-carrier noise of the slave laser and the noise from the master laser still contribute to the noise in the P1 dynamics. Therefore, for white noise associated with the master and slave lasers the various LS operating points show more complex noise suppression characteristics. The noise-cancelling properties of the P1 oscillation frequency induced by an optically injected semiconductor laser subject to simultaneous fluctuation noise terms is beyond the scope of this work.

These characteristics of the various LS operating points can be a guide to be exploited in the P1 oscillation stabilization schemes to further suppress the effects of unwanted system fluctuations. The optically injected semiconductor laser displays broadband insensitivity of the P1 oscillation frequency against system noise, which compares favorably to other photonic microwave oscillators for emerging photonic microwave applications.

REFERENCES

[1] S. Strogatz, *Nonlinear Dynamics and Chaos with Student Solutions Manual: With Applications to Physics, Biology, Chemistry, and Engineering*. Boulder, CO, USA: Westview Press, 2000.

[2] S. Wieczorek, B. Krauskopf, T. B. Simpson, and D. Lenstra, "The dynamical complexity of optically injected semiconductor lasers," *Phys. Rep.*, vol. 416, pp. 1–128, Sep. 2005.

[3] S.-C. Chan, S.-K. Hwang, and J.-M. Liu, "Period-one oscillation for photonic microwave transmission using an optically injected semiconductor laser," *Opt. Express*, vol. 15, no. 22, pp. 14921–14935, Oct. 2007.

[4] C.-H. Chu, S.-L. Lin, S.-C. Chan, and S.-K. Hwang, "All-optical modulation format conversion using nonlinear dynamics of semiconductor lasers," *IEEE J. Quantum Electron.*, vol. 48, no. 11, pp. 1389–1396, Nov. 2012.

[5] Y.-H. Hung, C.-H. Chu, and S.-K. Hwang, "Optical double-sideband modulation to single-sideband modulation conversion using period-one nonlinear dynamics of semiconductor lasers for radio-over-fiber links," *Opt. Lett.*, vol. 38, no. 9, pp. 1482–1484, 2013.

[6] Y.-H. Hung, C.-H. Tseng, and S.-K. Hwang, "Conversion from non-orthogonally to orthogonally polarized optical single-sideband modulation using optically injected semiconductor lasers," *Opt. Lett.*, vol. 43, no. 11, pp. 2628–2631, 2018.

[7] C. Cui and S.-C. Chan , "Performance analysis on using period-one oscillation of optically injected semiconductor lasers for radio-over-fiber uplinks," *IEEE J. Quantum Electron.*, vol. 48, no. 4, pp. 490–499, Apr. 2012.

[8] Y. Liu, X. Qi, and L. Xie, "Dual-beam optically injected semiconductor laser for radio-over-fiber downlink transmission with tunable microwave subcarrier frequency," *Opt. Commun.*, vol. 292, pp. 117–122, Apr. 2013.

[9] C.-H. Cheng, C.-W. Lee, T.-W. Lin, and F.-Y. Lin, "Dual-frequency laser Doppler velocimeter for speckle noise reduction and coherence enhancement," *Opt. Express*, vol. 20, no. 18, pp. 20255–20265, 2012.

[10] S.-C. Chan, R. Diaz, and J.-M. Liu, "Novel photonic applications of nonlinear semiconductor laser dynamics," *Opt. Quantum Electron.*, vol. 40, pp. 83–95, Mar. 2008.

[11] S.-K. Hwang, J.-M. Liu, and J. K. White, "Characteristics of period-one oscillations in semiconductor lasers subject to optical injection," *IEEE J. Sel. Topics Quantum Electron.*, vol. 10, no. 5, pp. 974–981, Sep. 2004.

[12] A. Hurtado, A. Quirce, A. Valle, L. Pesquera, and M. J. Adams, "Nonlinear dynamics induced by parallel and orthogonal optical injection in 1550 nm vertical-cavity surface-emitting lasers (VCSELs)," *Opt. Express*, vol. 18, no. 9, pp. 9423–9428, Apr. 2010.

[13] A. Hurtado, J. Mee, M. Nami, I. D. Henning, M. J. Adams, and L. F. Lester, "Tunable microwave signal generator with an optically-injected 1310nm QD-DFB laser," *Opt. Express*, vol. 21, no. 9, pp. 10772–10778, 2013.

[14] T. Erneux, V. Kovanis, and A. Gavrielides, "Nonlinear dynamics of an injected quantum cascade laser," *Phys. Rev. E, Stat. Phys. Plasmas Fluids Relat. Interdiscip. Top.*, vol. 88, Sep. 2013, Art. no. 032907.

[15] Z. A. Sattar, N. A. Kamel, and K. A. Shore, "Optical injection effects in nanolasers," *IEEE J. Quantum Electron.*, vol. 52, no. 2, pp. 1–8, Feb. 2016.

[16] X.-Q. Qi and J.-M. Liu, "Photonic microwave applications of the dynamics of semiconductor lasers," *IEEE J. Sel. Topics Quantum Electron.*, vol. 17, no. 5, pp. 1198–1211, Sep. 2011.

[17] J.-P. Zhuang and S.-C. Chan, "Phase noise characteristics of microwave signals generated by semiconductor laser dynamics," *Opt. Express*, vol. 23, no. 3, pp. 2777–2797, 2015.

[18] T. B. Simpson, J.-M. Liu, M. AlMulla, N. G. Usechak, and V. Kovanis, "Linewidth sharpening via polarization-rotated feedback in optically injected semiconductor laser oscillators," *IEEE J. Sel. Topics Quantum Electron.*, vol. 19, no. 4, Aug. 2013, Art. no. 1500807.

[19] T. B. Simpson and F. Doft, "Double-locked laser diode for microwave photonics applications," *IEEE Photon. Technol. Lett.*, vol. 11, no. 11, pp. 1476–1478, Nov. 1999.

[20] M. AlMulla, "Optical double-locked semiconductor lasers," *Results Phys.*, vol. 9, pp. 63–70, Jun. 2018.

[21] Y. H. Hung and S. K. Hwang, "Photonic microwave stabilization for period-one nonlinear dynamics of semiconductor lasers using optical modulation sideband injection locking," *Opt. Express*, vol. 23, no. 5, pp. 6520–6532, 2015.

[22] S.-C. Chan and J.-M. Liu, "Tunable narrow-linewidth photonic microwave generation using semiconductor laser dynamics," *IEEE J. Sel. Topics Quantum Electron.*, vol. 10, no. 5, pp. 1025–1032, Sep. 2004.

[23] J. S. Suelzer, T. B. Simpson, P. Devgan, and N. G. Usechak, "Tunable, low-phase-noise microwave signals from an optically injected semiconductor laser with opto-electronic feedback," *Opt. Lett.*, vol. 42, no. 16, pp. 3181–3184, 2017.

[24] J.-P. Zhuang and S.-C. Chan, "Tunable photonic microwave generation using optically injected semiconductor laser dynamics with optical feedback stabilization," *Opt. Lett.*, vol. 38, no. 3, pp. 344–346, 2013.

[25] T. B. Simpson, J.-M. Liu, M. AlMulla, N. G. Usechak, and V. Kovanis, "Limit-cycle dynamics with reduced sensitivity to perturbations," *Phys. Rev. Lett.*, vol. 112, Jan. 2014, Art. no. 023901.

[26] M. AlMulla and J.-M. Liu, "Frequency-stabilized limit-cycle dynamics of an optically injected semiconductor laser," *Appl. Phys. Lett.*, vol. 105, Jul. 2014, Art. no. 011122.

[27] M. AlMulla and J.-M. Liu, "Stable periodic dynamics of reduced sensitivity to perturbations in optically injected semiconductor lasers," *IEEE J. Sel. Topics Quantum Electron.*, vol. 21, no. 6, pp. 1–8, Dec. 2015.
[28] T. B. Simpson, J.-M. Liu, M. AlMulla, N. G. Usechak, and V. Kovanis, "Tunable oscillations in optically injected semiconductor lasers with reduced sensitivity to perturbations," *J. Lightw. Technol.*, vol. 32, no. 20, pp. 3749–3758, Oct. 1, 2014.
[29] J.-P. Zhuang, X.-Z. Li, S.-S. Li, and S.-C. Chan, "Frequency-modulated microwave generation with feedback stabilization using an optically injected semiconductor laser," *Opt. Lett.*, vol. 41, no. 24, pp. 5764–5767, 2016.
[30] Y.-N. Li, L. Fan, G.-Q. Xia, and Z.-M. Wu, "Tunable and broadband microwave frequency comb generation using optically injected semiconductor laser nonlinear dynamics," *IEEE Photon. J.*, vol. 9, no. 5, pp. 1–7, Oct. 2017.
[31] S.-C. Chan and J.-M. Liu, "Frequency modulation on single sideband using controlled dynamics of an optically injected semiconductor laser," *IEEE J. Quantum Electron.*, vol. 42, no. 7, pp. 699–705, Jul. 2006.
[32] T. B. Simpson, "Mapping the nonlinear dynamics of a distributed feedback semiconductor laser subject to external optical injection," *Opt. Commun.*, vol. 215, nos. 1–3, pp. 135–151, Jan. 2003.
[33] M. AlMulla and J.-M. Liu, "Effects of the gain saturation factor on the nonlinear dynamics of optically injected semiconductor lasers," *IEEE J. Quantum Electron.*, vol. 50, no. 3, pp. 158–165, Mar. 2014.
[34] S. K. Hwang, J. M. Liu, and J. K. White, "35-GHz intrinsic bandwidth for direct modulation in 1.3-um semiconductor lasers subject to strong injection locking," *IEEE Photon. Technol. Lett.*, vol. 16, no. 6, pp. 972–974, Apr. 15, 2004.
[35] J.-M. Liu and T. B. Simpson, "Four-wave mixing and optical modulation in a semiconductor laser," *IEEE J. Quantum Electron.*, vol. 30, no. 4, pp. 957–965, Apr. 1994.
[36] T. B. Simpson, F. Doft, E. Strzelecka, J. J. Liu, W. Chang, and G. J. Simonis, "Gain saturation and the linewidth enhancement factor in semiconductor lasers," *IEEE Photon. Technol. Lett.*, vol. 13, no. 8, pp. 776–778, Aug. 2001.
[37] M. AlMulla, "Optimizing optically injected semiconductor lasers for periodic dynamics with reduced sensitivity to perturbations," *Opt. Express*, vol. 27, no. 12, pp. 17283–17297, 2019.

MOHAMMAD A. ALMULLA received the B.S. degree in electrical engineering from Kuwait University, Kuwait, in 2008, and the M.S. and Ph.D. degrees in electrical engineering from the University of California, Los Angeles, CA, USA, in 2012 and 2015, respectively.

He is currently an Assistant Professor of electrical engineering with Kuwait University. His current research interests include optical communication systems, microwave photonics, semiconductor lasers, and nonlinear dynamics.

JIA-MING LIU (M'83–SM'85–F'08–LF'19) received the B.S. degree in electrophysics from National Chiao Tung University, Hsinchu, Taiwan, in 1975, and the M.S. and Ph.D. degrees in applied physics from Harvard University, Cambridge, MA, USA, in 1979 and 1982, respectively.

He became a Licensed Professional Electrical Engineer, in 1977. He was an Assistant Professor with the Department of Electrical and Computer Engineering, State University of New York at Buffalo, Buffalo, NY, USA, from 1982 to 1983. He was a Senior Member of the Technical Staff of GTE Laboratories, Waltham, MA, USA, from 1983 to 1986. He joined the faculty of the Electrical Engineering Department, University of California, Los Angeles, CA, USA, in 1986. He is currently a Distinguished Professor of electrical and computer engineering and the Associate Dean for Academic Personnel of the Henry Samueli School of Engineering and Applied Science, University of California. He has pioneered a number of research areas, including the ultrafast laser–matter interactions, wavelength-tunable ultrashort laser pulses, nonlinear laser dynamics, laser chaos, chaotic optical communications, chaotic radar and lidar, and photonic microwave generation. His current research interests also cover nanophotonic imaging, neurophotonics, and graphene photonics. He has published over 250 scientific papers and 14 book chapters. He holds 12 U.S. patents. He has co-edited the book *Digital Communications Using Chaos and Nonlinear Dynamics* (Springer, 2006). He has authored or coauthored three books, namely the *Photonic Devices* (Cambridge University Press, 2005), the *Principles of Photonics* (Cambridge University Press, 2016), and the *Graphene Photonics* (Cambridge University Press, 2019). He is a Fellow of the American Physical Society, the Optical Society of America, and the Guggenheim Foundation.